

Superconductivity in the regime of attractive interactions in the Tomonaga-Luttinger liquid

Ž. Gosar,^{1,2} N. Janša,¹ T. Arh,¹ P. Jeglič,¹ M. Klanjšek,¹ H. F. Zhai,³ B. Lv,³ and D. Arčon^{1,2,*}

¹*Institute Jožef Stefan, Jamova c. 39, 1000 Ljubljana, Slovenia*

²*Faculty of mathematics and physics, University of Ljubljana, Jadranska c. 19, 1000 Ljubljana, Slovenia*

³*The University of Texas at Dallas, 800 West Campbell Road Richardson, Texas 75080-3021, USA*

While the vast majority of known physical realizations of the Tomonaga-Luttinger liquid (TLL) have repulsive interactions defined with the dimensionless interaction parameter $K_c < 1$, we here report that $\text{Rb}_2\text{Mo}_3\text{As}_3$ is in the opposite TLL regime of attractive interactions. This is concluded from a TLL-characteristic power-law temperature dependence of the ^{87}Rb spin-lattice relaxation rates over broad temperature range yielding the TLL interaction parameter for charge collective modes $K_c = 1.4$. The TLL of the one-dimensional band can be traced almost down to $T_c = 10.4$ K, where the bulk superconducting state is stabilized by the presence of a three-dimensional band and characterized by the ^{87}Rb temperature independent Knight shift and the absence of Hebel-Slichter coherence peak in the relaxation rates. The small superconducting gap measured in high magnetic fields reflects either the importance of the vortex core relaxation or the uniqueness of the superconducting state stemming from the attractive interactions defining the precursor TLL.

A universal paradigm of the Tomonaga-Luttinger liquid (TLL) [1–6] describes the physics of interacting fermions in one dimension remarkably well and predicts their most characteristic features that can be directly verified in experiments: collective excitations which generally separate into spin and charge modes and a power-law decay of the spin and charge correlation functions at long distances that lead to power-law dependencies of the corresponding experimental quantities as a function of temperature or frequency. Experimentally, such power-law dependencies were taken as a hallmark of TLL physics in molecular conductors such as tetrathiafulvalenetetracyanoquinodimethane TTF-TCNQ or Bechgaard salts $(\text{TMTSF})_2\text{X}$, where TMTSF denotes tetramethyltetraselenafulvalene [7], carbon nanotubes [8, 9] and in one-dimensional antiferromagnetic insulators [10–12].

These physical realizations of the TLL may be very diverse, but their behavior is universal as the extracted power-law exponents are functions of only the TLL parameter K , which characterizes the sign and the strength of interactions between collective excitation modes [1]. While the interactions in the TLLs are generally repulsive with $K < 1$, the only example of attractive interactions with $K > 1$ has been found in the quantum spin ladder system $(\text{C}_7\text{H}_{10}\text{N})_2\text{CuBr}_4$ [10, 13]. In one-dimensional metals, K depends on the strength of various scattering processes [14], which also define the competing orders: charge density wave, spin density wave or superconductivity. Remarkably, both the singlet and the triplet superconducting fluctuations are predicted [1–5] in the regime of attractive interactions. The emerging superconductivity in the $K > 1$ regime thus remains experimentally unexplored.

Here we focus on an intriguing class of solids, which are derived from the self-assembly of chains with inherently weak interchain coupling. Molybdenum-chalcogenide $(\text{Li}_x\text{MoS}_2, \text{Na}_{2-\delta}\text{Mo}_6\text{Se}_6)$ and molybdenum-oxide

$(\text{Li}_{0.9}\text{Mo}_6\text{O}_{17})$ chains [15–18] display many unusual properties associated with TLLs, but they also show a high degree of disorder due to the intercalation of metallic atoms between the chains. The disorder effects seem to be less important in Cr-pnictide quasi-one-dimensional metals, e.g., $\text{A}_2\text{Cr}_3\text{As}_3$ ($\text{A}=\text{K}, \text{Rb}, \text{Cs}$) with Cr_3As_3 chains as main building units, which remarkably also show low-temperature superconductivity with the critical temperature $T_c \approx 5$ K [19–27]. There seems to be a growing consensus for the unconventional singlet superconducting states in this family of materials based on the large specific-heat jump at T_c and large upper critical fields exceeding Pauli limit [19, 28], absence of the Hebel-Slichter coherence peak and the power-law dependence of nuclear spin-lattice relaxation rates, $1/T_1$, [22, 26] and the penetration depth proportional to temperature [23] that implies the nodal-type of a superconducting gap. Moreover, a possible ferromagnetic quantum critical point has been proposed based on variation of $1/T_1$ with the Cr-As-Cr angle [29]. However, the complicated electronic structure comprising two quasi-one-dimensional (1D) and one three-dimensional (3D) Fermi surface [30] and the presence of a Korringa component in the $1/T_1$ cast some doubts on the direct applicability of the TLL model for $\text{A}_2\text{Cr}_3\text{As}_3$ [22].

Recently, superconductivity has been discovered in $\text{K}_2\text{Mo}_3\text{As}_3$ made of assembled Mo_3As_3 chains (Fig. 1a) with a relatively high zero-field $T_c(0) = 10.4$ K [31]. Although $\text{A}_2\text{Mo}_3\text{As}_3$ are isostructural to their Cr counterparts $\text{A}_2\text{Cr}_3\text{As}_3$ and the first principle calculations suggest that they share similar electronic structure [32], the $4d$ character of electrons and stronger spin-orbit coupling may separate this family of superconductors into its own class. Here we report on the normal and superconducting state in $\text{Rb}_2\text{Mo}_3\text{As}_3$ and find some fundamental differences with respect to the family of $\text{A}_2\text{Cr}_3\text{As}_3$. Strikingly, the TLL of the 1D components of the Fermi surface

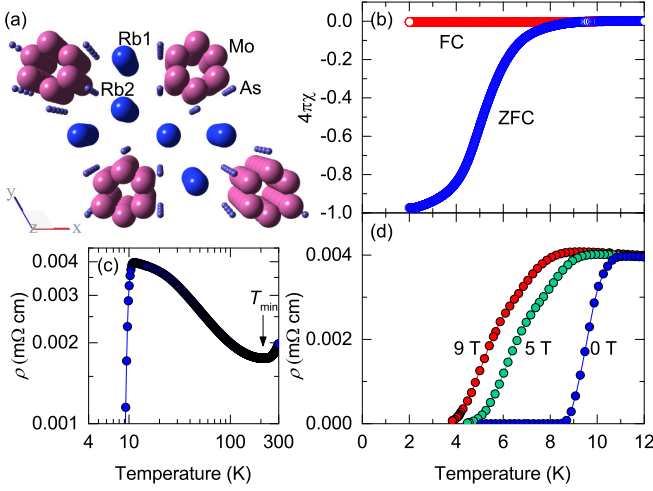


FIG. 1. (a) The assembly of Mo_3As_3 chains in the $\text{Rb}_2\text{Mo}_3\text{As}_3$ structure. Large pink spheres stand for Mo atoms whereas small violet spheres for As atoms. Rb atoms (large blue spheres) are in the two different crystallographic positions Rb1 ($3k$) and Rb2 ($1c$). (b) Temperature dependence of static spin susceptibility of $\text{Rb}_2\text{Mo}_3\text{As}_3$ measured under the zero-field-cooled (blue) and the field-cooled (red) protocols at $\mu_0 H = 1$ mT. (c) Temperature dependence of zero-field resistivity $\rho(T)$ (blue circles) showing a superconducting transition at $T_c(0) = 10.4$ K. (d) Low-temperature resistivities measured in zero-field (blue), 5 T (green) and 9 T (red).

in which effective attractive interactions between collective charge excitations prevail can be followed in ^{87}Rb nuclear magnetic resonance (NMR) experiments over an extremely broad temperature range from ~ 200 K almost down to T_c . On the other hand, ^{75}As nuclei couple more strongly to the 3D band. Directly from such a multi-orbital state, superconductivity develops, but the insensitivity of the ^{87}Rb Knight shift to the onset of the superconducting state, the absence of Hebel-Slichter coherence peak and the reduced superconducting gap in a moderate field imply its unconventional character.

Powder samples of $\text{Rb}_2\text{Mo}_3\text{As}_3$ were prepared via standard high-temperature solid state method previously used to synthesize $\text{A}_2\text{Cr}_3\text{As}_3$ samples [20, 27]. Powder X-ray diffraction measurements show phase pure sample with the $\text{A}_2\text{Cr}_3\text{As}_3$ -type structure – hexagonal crystal lattice with a space group of $P\bar{6}m2$ [19]. The sample was further investigated by dc magnetic susceptibility measurements in the zero-field-cooled (ZFC) and field-cooled (FC) modes at $\mu_0 H = 1$ mT (Fig. 1b). The $\text{Rb}_2\text{Mo}_3\text{As}_3$ compound indeed shows a bulk superconductivity below zero-field $T_c(0) \approx 10$ K with the large diamagnetic shielding $4\pi\chi_{\text{ZFC}}$ of 97% at 2 K demonstrating sample's high quality. Next, the temperature dependence of the zero-field resistivity, $\rho(T)$, was measured (Fig. 1c) using Quantum Design Physical Property Measurement System (PPMS) system. The resistivity at high temperatures decreases with decreasing temperature, with a min-

imum at $T_{\min} \sim 210$ K where $\rho(T)$ starts to increase with decreasing temperature. Just above $T_c(0) = 10.4$ K, $\rho(T)$ first almost flattens as a function of temperature and then it sharply drops to zero where the superconducting state sets in. The normal-state increase in $\rho(T)$ with decreasing temperature below T_{\min} may imply the weak localization effects due to the presence of disorder and Coulomb repulsion [2, 16]. Measurements of $\rho(T)$ in the magnetic field show a suppression of superconductivity and the corresponding decrease of T_c with increasing magnetic field (Fig. 1d). In the field of 9 T, the critical temperature decreases to $T_c \approx 8$ K. The magnetization and resistivity data thus confirm the high quality of the sample and the emerging superconducting state, but could not resolve alone on the potential TLL physics in this material nor on the symmetry of the superconducting state.

We thus turn to ^{87}Rb (nuclear spin $I = 3/2$) NMR, which was measured in magnetic fields of 4.7 T and 9.39 T with the corresponding reference Larmor frequencies of $\nu_L = 65.442$ MHz and 130.871 MHz, respectively. We note that Rb atoms are intercalated into the voids between the Mo_3As_3 chains (Fig. 1a) and thus couple to the intrinsic intra-chain low-energy dynamics through the contributions of the Mo $4d$ bands that cross the Fermi energy [32]. The ^{87}Rb NMR spectrum measured in 9.39 T (Fig. 2a) is composed of a narrow peak corresponding to the central $1/2 \leftrightarrow -1/2$ transition, which is shifted for ~ 56 kHz with respect to the ν_L , and the two broadened satellite peaks that symmetrically flank the central one and which yield the quadrupole frequency $\nu_Q \approx 280$ kHz. The second-order quadrupole shift of the central transition line, $\delta\nu \propto \nu_Q^2/\nu_L$, is thus small. The measured line shift must therefore come almost entirely from the hyperfine coupling to the itinerant electrons, *i.e.*, the Knight shift K_{87} . In addition to this ^{87}Rb resonance, we find also a broader component with a small shift and whose satellite transitions cannot be resolved (Fig. 2a). The two-component NMR spectrum reflects two crystallographic Rb sites (at the $3k$ and $1c$ positions [19], Fig. 1a), where only one of them (probably Rb1 at the $3k$ positions) strongly couples to the Mo_3As_3 chains. The analogous two-component ^{133}Cs NMR spectrum has been observed also in $\text{Cs}_2\text{Cr}_3\text{As}_3$ [22].

The central transition Rb1 peak strongly shifts with temperature between room temperature and $T = 50$ K and then becomes almost temperature independent between 50 K and T_c . Since the Knight shift, $K_{87} = \frac{a_{\text{Rb}}}{N_A \mu_B} \chi(T)$ (here a_{Rb} , N_A and μ_B are the ^{87}Rb hyperfine coupling constant, the Avogadro number and the Bohr magneton, respectively), is directly proportional to the contribution to the static spin susceptibility from a band that dominantly couples to ^{87}Rb , we conclude that associated intrinsic susceptibility $\chi(T)$ is also significantly temperature dependent. This would be highly unusual for the Pauli susceptibility of the Fermi liquid in two- and three-dimensions. On the other hand, large and tem-

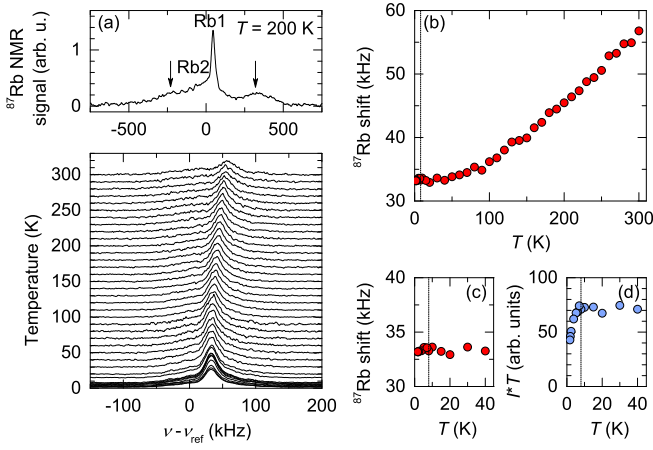


FIG. 2. (a) ^{87}Rb NMR spectra in $\text{Rb}_2\text{Mo}_3\text{As}_3$ powder. Top: the full spectrum measured at $T = 200$ K. Arrows indicate the two satellite transitions at $\pm\nu_Q$ relative to the Rb1-site central transition. The region of the non-shifted Rb2 component is also indicated. Bottom: the full temperature dependence of the Rb1 central transition line. (b) Temperature dependence of the ^{87}Rb NMR shift for Rb1 site. (c) Temperature dependencies close to T_c for the ^{87}Rb NMR shift and (d) for the integrated signal intensity multiplied by temperature. $T_c \approx 8$ K (dashed vertical lines) in the NMR field of 9.39 T.

perature dependent $\chi(T)$ is not uncommon to 1D metals [15]. Calculations for the Hubbard model of interacting electrons in 1D in fact predict a maximum in $\chi(T)$ at $T \sim 0.18t$ (t is the hopping matrix element) followed by an inflection at $T \sim 0.1t$ [33]. While the comparison between the experimental and theoretical data can be at this stage only at a qualitative level, the temperature dependent K_{87} implies the dominant coupling of ^{87}Rb to the 1D bands and explains why K_{87} does not follow bulk spin susceptibility (Fig. S1 in [34]) with contributions from both 1D and 3D bands [32].

In order to quantitatively discuss the possible TLL physics, we switch to the ^{87}Rb $1/T_1$ (Fig. 3), which is proportional to the sum of the imaginary part of the electron spin susceptibility $\chi''(q, \omega_L)$ over the wave vector q and calculated at $\omega_L = 2\pi\nu_L$: $1/T_1 T \propto \sum_q |a_{\text{Rb}}(q)|^2 \frac{\chi''(q, \omega_L)}{\omega_L}$. This makes $1/T_1$ an extremely sensitive probe of the low-energy dynamics. $1/T_1$ has a weakly pronounced field-dependent maximum at $T \sim 250$ K (Fig. S2 in [34]), which coincides with the minimum in $\rho(T)$ and indicates the freezing out of the Rb^+ ion dynamics, most probably of Rb at the 1c position where the alkali metal vacancies are primarily located [35]. However, once such dynamics is completely frozen on the time-scale of ω_L below 200 K, a clear power-law temperature dependence of $1/T_1 \propto T^p$ is observed in 4.7 T and 9.39 T over more than a decade in temperature between ~ 10 K and 200 K. This is a signal that the low-energy dynamics is described by the critical phenomena of collective modes and is thus a hallmark of the TLL where the quantum

critical regime is universal. $1/T_1 T$ shows no contribution from the ferromagnetic spin fluctuations similar to those recently reported for the superconducting $\text{A}_2\text{Cr}_3\text{As}_3$ [29]. Finally, $1/T_1$ data does not follow the Fermi-liquid-type Korringa relaxation $1/T_1 T \propto K_{87}^2$ either (Fig. S3 in [34]), which implies that the 3D part of the Fermi surface has a negligible contribution to the ^{87}Rb $1/T_1$. The ^{87}Rb $1/T_1$ is thus completely dominated by the two 1D bands, which are responsible for the TLL behavior. On the other hand, zero-field ^{75}As $1/T_1$ nuclear quadrupole resonance (NQR) measurements (Figs. S4 and S5 in [34]) show $1/T_1 \propto T$ (Fig. 3) and suggest that ^{75}As sitting in the Mo_3As_3 chains predominantly couple to the part of the Fermi surface with a 3D character. Combined ^{87}Rb and ^{75}As $1/T_1$ thus corroborate multi-band physics [32] and the interplay of 1D and 3D bands in the studied system.

The power-law fit of ^{87}Rb $1/T_1$ yields $p \approx 1.4$ for both 4.7 T and 9.39 T measurements. This is dramatically different from $p \approx 0.75$, determined in $\text{K}_2\text{Cr}_3\text{As}_3$ [26] or $p = 0.34$ in single-wall carbon nanotubes [9] and immediately suggests that the 1D bands of $\text{Rb}_2\text{Mo}_3\text{As}_3$ are in a different TLL regime. In general, TLL is described by separate spin and charge collective modes, described by the corresponding TLL interaction parameters K_s and K_c , respectively. Assuming the spin invariance in low fields, which gives $K_s = 1$, we focus only on the charge mode, which is affected by the interactions [36]. For the single-band TLL case, $1/T_1 T \propto T^{\eta/2-2}$ is predicted, where $\eta = 2K_c + 2$ holds the information about the TLL parameter for the $2k_F$ spin fluctuations. From the experiment we get $K_c = p = 1.4$, which puts the studied system into the regime with dominant attractive interactions. The more general treatment of the case of two 1D bands has been developed in the context of single-wall carbon nanotubes [36]. The number of charge and spin excitation modes doubles and thus additional independent measurements are required to extract all the TLL parameters [9]. We stress though, that the simple one-band TLL limit is valid also for two-band system, if the two corresponding charge modes are decoupled. Regardless of these uncertainties, the finding that $K_c > 1$ is important because it demonstrates for $\text{Rb}_2\text{Mo}_3\text{As}_3$ that the effective interactions are attractive. This opens a path to superconductivity, whether with singlet or triplet symmetry even in the presence of weak disorder, depending on the strength of the scattering processes [2–5].

The onset of superconductivity below $T_c \approx 8$ K is barely seen in the line shift of the ^{87}Rb NMR spectra measured in 9.39 T (Fig. 2c), but can be deduced from the wipeout effect (Fig. 2d). In the temperature dependence of ^{87}Rb $1/T_1$, the onset of superconductivity is seen as a sudden suppression of $1/T_1$ (Fig. 4a) without any Hebel-Slichter coherence peak, which would be a hallmark of the conventional Bardeen-Cooper-Schrieffer (BCS) s-wave superconductivity, but is common to

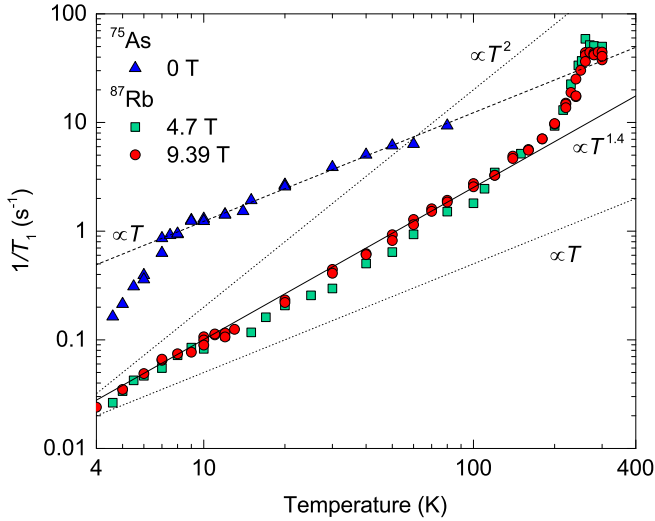


FIG. 3. Temperature dependence of the zero-field ^{75}As (blue triangles) and ^{87}Rb $1/T_1$ measured in 4.7 T (green squares) and 9.39 T (red circles) for the $\text{Rb}_2\text{Mo}_3\text{As}_3$ powder. The power-law dependence $1/T_1 \propto T^p$ with $p = 1.4$ (solid line) for ^{87}Rb data demonstrates the TLL physics of 1D bands. For comparison, linear and quadratic dependencies are denoted with dotted lines, respectively. ^{75}As nuclei, which are predominantly coupled to the 3D electronic band, show the conventional $1/T_1 \propto T$ behavior (dashed line).

unconventional superconductors, including related iron-pnictide superconductors [37] and $\text{A}_2\text{Cr}_3\text{As}_3$ [26, 29]. In $\text{Rb}_2\text{Mo}_3\text{As}_3$, $1/T_1$ apparently follows an activated temperature dependence, $1/T_1 \propto \exp(-\Delta_0/k_B T)$ down to $T_c/T = 2.7$ (Fig. 4b). Attempts to fit $1/T_1$ to the power law T^n for $T_c > T > T_c/2.7$ with $n \sim 3 - 5$ result in a worse fit. We thus employ $1/T_1 \propto \exp(-\Delta_0/k_B T)$ to estimate the superconducting gap $\Delta_0 \approx 0.9$ meV (Fig. 4b and Table SI in [34]). Using $T_c \approx 8$ K deduced from the onset of superconductivity in $\rho(T)$ (Fig. 1d), we can then calculate the energy gap- T_c ratio $2\Delta_0/k_B T_c = 2.4$, well below the standard BCS value of $2\Delta_0/k_B T_c \geq 3.52$. Equivalent analysis and conclusions hold also for measurements in 4.7 T. Remarkably, the temperature dependence of the zero-field $1/T_1$ for the ^{75}As , which couples to the 3D part of the Fermi surface, can still be described by the thermally activated dependence without Hebel-Slichter coherence peak, but with a larger $\Delta_0 = 1.6$ meV and $2\Delta_0/k_B T_c = 3.7$.

Complementary ^{87}Rb NMR and ^{75}As NQR data reveal that $\text{Rb}_2\text{Mo}_3\text{As}_3$ has to be treated as a multiband system comprising 1D and 3D bands. It is thus reasonable to assume a two-gap scenario for the superconductivity. However, such a two-gap scenario could not easily explain the difference between the extracted $2\Delta_0/k_B T_c$ from the ^{75}As and ^{87}Rb data and could be seen if the gap averaging due to impurity scattering is weak [38]. As the resistivity data (Fig. 1c) indicate the presence of disorder, such an interpretation of the NMR and NQR data

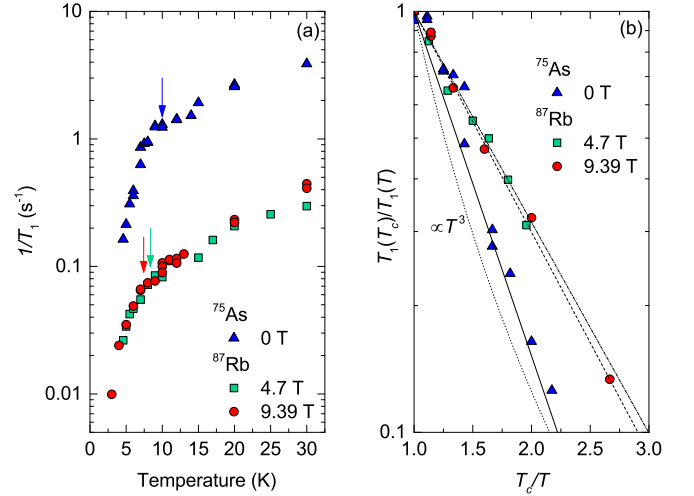


FIG. 4. (a) Temperature dependence of ^{87}Rb $1/T_1$ for $\text{Rb}_2\text{Mo}_3\text{As}_3$ measured in 4.7 T (green squares) and 9.39 T (red circles) close to T_c . Blue triangles stand for the zero-field ^{75}As $1/T_1$ values. Vertical arrows mark the superconducting transition temperatures. (b) Normalized ^{87}Rb relaxation rates, $T_1(T_c)/T_1(T)$, vs inverse temperature, T_c/T , in 4.7 T (green squares) and 9.39 T (red circles). For comparison, zero-field ^{75}As $T_1(T_c)/T_1(T)$ is also shown (blue triangles). Dashed lines are fits of ^{87}Rb $1/T_1$ to an activated temperature dependence yielding $2\Delta_0/k_B T_c \approx 2.4$, while solid line is a fit of ^{75}As $1/T_1$ to the same model with $2\Delta_0/k_B T_c \approx 3.7$ (Table SI in [34]). $1/T_1 \propto T^3$ dependence is shown by a dotted line.

is less likely to apply to $\text{Rb}_2\text{Mo}_3\text{As}_3$. On the other hand, the smallness of the extracted Δ_0 for the ^{87}Rb NMR may result from the vortex core relaxation [39]. In this case, the measured ^{87}Rb NMR $1/T_1$ is a weighted average of the relaxation in the vortex core and in the inter-vortex region. If that is the case, then we find the marginal difference between the 4.7 T and 9.39 T data fairly surprising.

The absence of a noticeable shift in ^{87}Rb NMR upon cooling through the superconducting transition (Fig. 2c) may imply the elusive spin-triplet superconductivity [40], which is compatible with the theoretical prediction of the triplet superconducting fluctuations [1–5] in the TLL regime of attractive interactions. Experimentally, the superconductivity should persist at fields exceeding the paramagnetic limit, as it was indeed previously observed in $\text{A}_2\text{Cr}_3\text{As}_3$ samples [19, 28]. However, in triplet superconductors, the power-law scaling of $1/T_1$ with $n \sim 3 - 5$ is expected [41], which has yet to be tested for $\text{Rb}_2\text{Mo}_3\text{As}_3$ with measurements to even lower temperatures. Finally, the extracted values of $2\Delta_0/k_B T_c$ may be affected also by the quenched disorder perturbing TLL near the superconductor-to-insulator transition leading to situations when the length scale of the inhomogeneity is comparable to or larger than the coherence length [42, 43]. In $\text{Rb}_2\text{Mo}_3\text{As}_3$, the source of disorder could be connected to the Rb^+ 1c sites, whereas the effective

attractive interactions within the TLL place this system very close to the metal(superconductor)-to-insulator critical point. The increase in $\rho(T)$ with decreasing temperature below T_{\min} (Fig. 1c) seems to corroborate this suggestion, but more experiments to even lower temperatures are needed to fully understand the relation between the disorder, the size and the sign of interactions defining the TLL and the emerging bulk superconductivity in the $A_2Mo_3As_3$ family.

In conclusion, we have studied $Rb_2Mo_3As_3$ composed of the assembly of weakly coupled Mo_3As_3 chains and have shown that the 1D bands adopt TLL behavior over a strikingly broad temperature range. A power-law dependence of ^{87}Rb $1/T_1$ demonstrates the realization of the TLL with $K_c > 1$ which has been rarely accessible before in realistic physical systems. The multiband electronic structure probed by ^{75}As and ^{87}Rb nuclei, the vortex core relaxation and the underlying TLL characterized by the effective attractive coupling are discussed in connection to the unusual superconductivity marked by the temperature independent Knight shift, the absence of the Hebel-Slichter coherence peak and the reduced superconducting gap.

Acknowledgements D.A. acknowledges the financial support of the Slovenian Research Agency through J1-9145 and P1-0125 grants. The work at UT Dallas is supported by US Air Force Office of Scientific Research (AFOSR) No. FA9550-15-1-0236 and FA9550-19-1-0037.

* denis.arcon@ijs.si

- [1] T. Giamarchi, *Quantum Physics in One Dimension*, International Series of Monographs on Physics (Clarendon Press, 2003).
- [2] T. Giamarchi and H. J. Schulz, Phys. Rev. B **37**, 325 (1988).
- [3] H. J. Schulz, G. Cuniberti, and P. Pieri, (1998), arXiv:cond-mat/9807366 [cond-mat.str-el].
- [4] S. Nishimoto, K. Sano, and Y. Ohta, Phys. Rev. B **77**, 085119 (2008).
- [5] J.-P. Pouget, Physica B: Condensed Matter **407**, 1762 (2012), Proceedings of the International Workshop on Electronic Crystals (ECRYS-2011).
- [6] K. Schönhammer, in *Strong interactions in low dimensions* (Springer, 2004) pp. 93–136.
- [7] D. Jerome and H. J. Schulz, Advances in Physics **51**, 293 (2002).
- [8] M. Bockrath, D. H. Cobden, J. Lu, A. G. Rinzler, R. E. Smalley, L. Balents, and P. L. McEuen, Nature **397**, 598 (1999).
- [9] Y. Ihara, P. Wzietek, H. Alloul, M. H. Rmmeli, T. Pichler, and F. Simon, Europhys. Lett. **90**, 17004 (2010).
- [10] M. Jeong, H. Mayaffre, C. Berthier, D. Schmidiger, A. Zheludev, and M. Horvatić, Phys. Rev. Lett. **111**, 106404 (2013).
- [11] M. Klanjšek, D. Arčon, A. Sans, P. Adler, M. Jansen, and C. Felser, Phys. Rev. Lett. **115**, 057205 (2015).
- [12] T. Knaflič, M. Klanjšek, A. Sans, P. Adler, M. Jansen, C. Felser, and D. Arčon, Phys. Rev. B **91**, 174419 (2015).
- [13] M. Jeong, D. Schmidiger, H. Mayaffre, M. Klanjšek, C. Berthier, W. Knafo, G. Ballon, B. Vignolle, S. Krämer, A. Zheludev, and M. Horvatić, Phys. Rev. Lett. **117**, 106402 (2016).
- [14] J. Solyom, Advances in Physics **28**, 201 (1979).
- [15] D. Mihailović, Z. Jagličić, D. Arčon, A. Mrzel, A. Zorko, M. Remškar, V. V. Kabanov, R. Dominko, M. Gaberšček, C. J. Gómez-García, J. M. Martínez-Agudo, and E. Coronado, Phys. Rev. Lett. **90**, 146401 (2003).
- [16] A. Petrović, D. Ansermet, D. Chernyshov, M. Hoesch, D. Salloum, P. Gougeon, M. Potel, L. Boeri, and C. Panagopoulos, Nat. Commun. **7**, 12262 (2016).
- [17] N. Wakeham, A. F. Bangura, X. Xu, J.-F. Mercure, M. Greenblatt, and N. E. Hussey, Nat. Commun. **2**, 396 (2011).
- [18] P. Chudzinski, T. Jarlborg, and T. Giamarchi, Phys. Rev. B **86**, 075147 (2012).
- [19] J.-K. Bao, J.-Y. Liu, C.-W. Ma, Z.-H. Meng, Z.-T. Tang, Y.-L. Sun, H.-F. Zhai, H. Jiang, H. Bai, C.-M. Feng, Z.-A. Xu, and G.-H. Cao, Phys. Rev. X **5**, 011013 (2015).
- [20] Z.-T. Tang, J.-K. Bao, Y. Liu, Y.-L. Sun, A. Ablimit, H.-F. Zhai, H. Jiang, C.-M. Feng, Z.-A. Xu, and G.-H. Cao, Phys. Rev. B **91**, 020506 (2015).
- [21] M. D. Watson, Y. Feng, C. W. Nicholson, C. Monney, J. M. Riley, H. Iwasawa, K. Refson, V. Sacksteder, D. T. Adroja, J. Zhao, and M. Hoesch, Phys. Rev. Lett. **118**, 097002 (2017).
- [22] H. Zhi, D. Lee, T. Imai, Z. Tang, Y. Liu, and G. Cao, Phys. Rev. B **93**, 174508 (2016).
- [23] G. M. Pang, M. Smidman, W. B. Jiang, J. K. Bao, Z. F. Weng, Y. F. Wang, L. Jiao, J. L. Zhang, G. H. Cao, and H. Q. Yuan, Phys. Rev. B **91**, 220502 (2015).
- [24] D. T. Adroja, A. Bhattacharyya, M. Telling, Y. Feng, M. Smidman, B. Pan, J. Zhao, A. D. Hillier, F. L. Pratt, and A. M. Strydom, Phys. Rev. B **92**, 134505 (2015).
- [25] D. Adroja, A. Bhattacharyya, M. Smidman, A. Hillier, Y. Feng, B. Pan, J. Zhao, M. R. Lees, A. Strydom, and P. K. Biswas, J. Phys. Soc. Jpn. **86**, 044710 (2017).
- [26] H. Z. Zhi, T. Imai, F. L. Ning, J.-K. Bao, and G.-H. Cao, Phys. Rev. Lett. **114**, 147004 (2015).
- [27] Q.-G. Mu, B.-B. Ruan, B.-J. Pan, T. Liu, J. Yu, K. Zhao, G.-F. Chen, and Z.-A. Ren, Phys. Rev. B **96**, 140504 (2017).
- [28] Z.-T. Tang, Y. Liu, J.-K. Bao, C.-Y. Xi, L. Pi, and G.-H. Cao, Journal of Physics: Condensed Matter **29**, 424002 (2017).
- [29] J. Luo, J. Yang, R. Zhou, Q. G. Mu, T. Liu, Z.-a. Ren, C. J. Yi, Y. G. Shi, and G.-q. Zheng, Phys. Rev. Lett. **123**, 047001 (2019).
- [30] A. Subedi, Phys. Rev. B **92**, 174501 (2015).
- [31] Q.-G. Mu, B.-B. Ruan, K. Zhao, B.-J. Pan, T. Liu, L. Shan, G.-F. Chen, and Z.-A. Ren, Science Bulletin **63**, 952 (2018).
- [32] Y. Yang, S.-Q. Feng, H.-Y. Lu, W.-S. Wang, and Z.-P. Chen, J. Supercond. Nov. Magn. (2019), 10.1007/s10948-019-5054-z.
- [33] H. Néglise, C. Bourbonnais, H. Touchette, Y. Vilks, and A.-M. Tremblay, The European Physical Journal B - Condensed Matter and Complex Systems **12**, 351 (1999).
- [34] “Supplemental material” .
- [35] J.-K. Bao, L. Li, Z.-T. Tang, Y. Liu, Y.-K. Li, H. Bai, C.-M. Feng, Z.-A. Xu, and G.-H. Cao, Phys. Rev. B **91**,

- 180404 (2015).
- [36] B. Dóra, M. Gulácsi, F. Simon, and H. Kuzmany, Phys. Rev. Lett. **99**, 166402 (2007).
 - [37] L. Ma and W.-Q. Yu, Chinese Physics B **22**, 087414 (2013).
 - [38] K. V. Samokhin and B. Mitrović, Phys. Rev. B **72**, 134511 (2005).
 - [39] A. Rigamonti, F. Borsa, and P. Carretta, Rep. Prog. Phys. **61**, 1367 (1998).
 - [40] I. J. Lee, S. E. Brown, W. G. Clark, M. J. Strouse, M. J. Naughton, W. Kang, and P. M. Chaikin, Phys. Rev. Lett. **88**, 017004 (2001).
 - [41] T. Rostunov, E. Demler, and A. Georges, Phys. Rev. Lett. **96**, 077002 (2006).
 - [42] J. M. Valles, R. C. Dynes, and J. P. Garno, Phys. Rev. Lett. **69**, 3567 (1992).
 - [43] Y. Zou, I. Klich, and G. Refael, Phys. Rev. B **77**, 144523 (2008).

Superconductivity in the regime of attractive interactions in the Tomonaga-Luttinger liquid

Supplemental Material

Ž. Gosar,^{1,2} N. Janša,¹ T. Arh,¹ P. Jeglič,¹ M. Klanjšek,¹ H. F. Zhai,³ B. Lv,³ and D. Arčon^{1,2,*}

¹*Institute Jožef Stefan, Jamova c. 39, 1000 Ljubljana, Slovenia*

²*Faculty of mathematics and physics, University of Ljubljana, Jadranska c. 19, 1000 Ljubljana, Slovenia*

³*The University of Texas at Dallas, 800 West Campbell Road Richardson, Texas 75080-3021, USA*

Nuclei	Magnetic field (T)	T_c (K)	Δ_0 (meV)	$2\Delta_0/k_B T_c$
^{75}As	0	10	1.62	3.7
^{87}Rb	4.7	9	0.89	2.4
^{87}Rb	9.39	8	0.83	2.4

TABLE I. Summary of fitting parameters for the spin-lattice relaxation rates in the superconducting state of $\text{Rb}_2\text{Mo}_3\text{As}_3$. The critical temperature T_c has been taken as an onset of the superconducting transition in the resistivity measurements (Fig. 1d in the main text), while the superconducting gap Δ_0 has been determined from the fits of the spin-lattice relaxation rates to the thermally activated behavior (Fig. 4b in the main text).

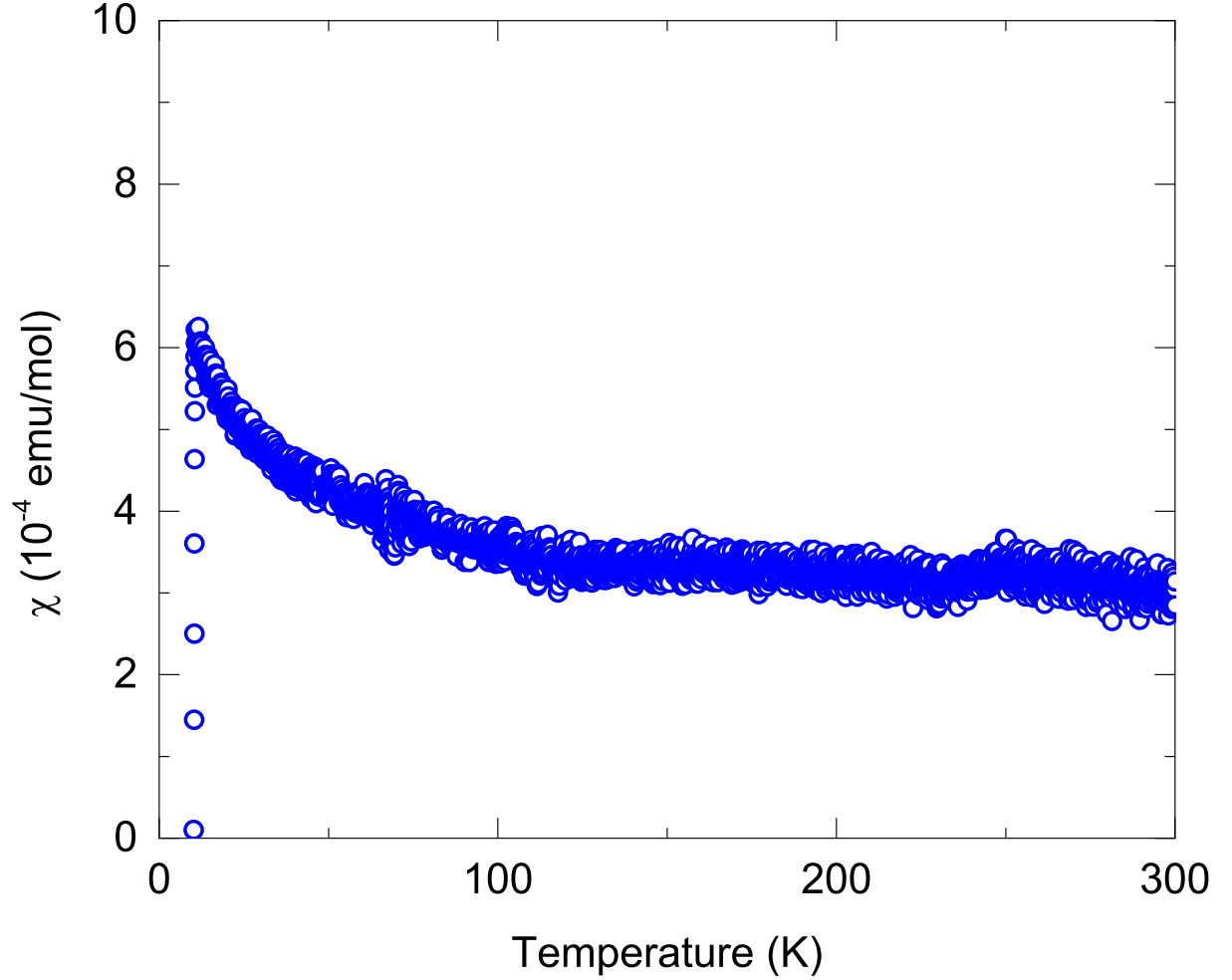


FIG. 1. Molar susceptibility of $\text{Rb}_2\text{Mo}_3\text{As}_3$ powder sample measured with the zero-field-cooling protocol and in the 0.1 T magnetic field. Quantum Design Physical Property Measurement System (PPMS) magnetometer has been used in these experiments.

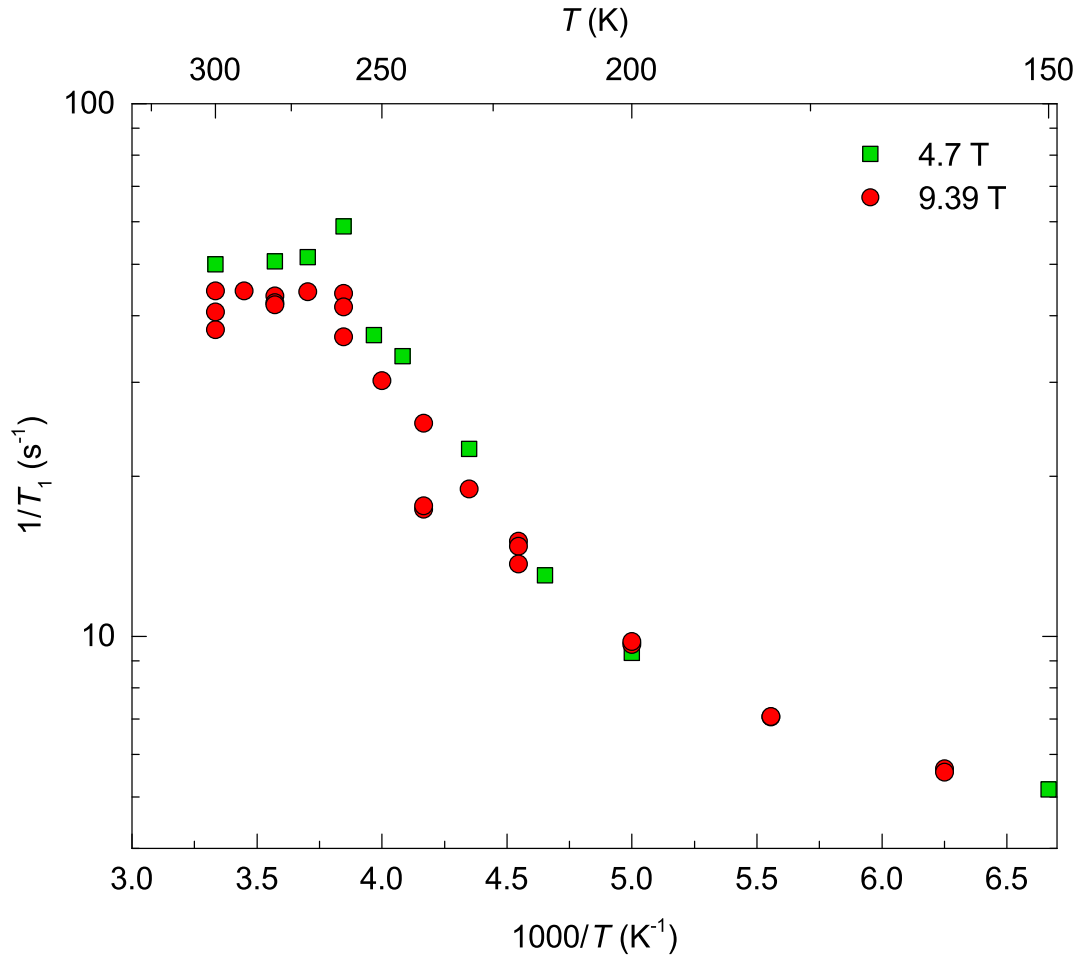


FIG. 2. ^{87}Rb $1/T_1$ measured in $\text{Rb}_2\text{Mo}_3\text{As}_3$ powder sample shows enhancement in a lower magnetic field around the maximum, which is expected for the Bloembergen-Purcell-Pound-type relaxation.

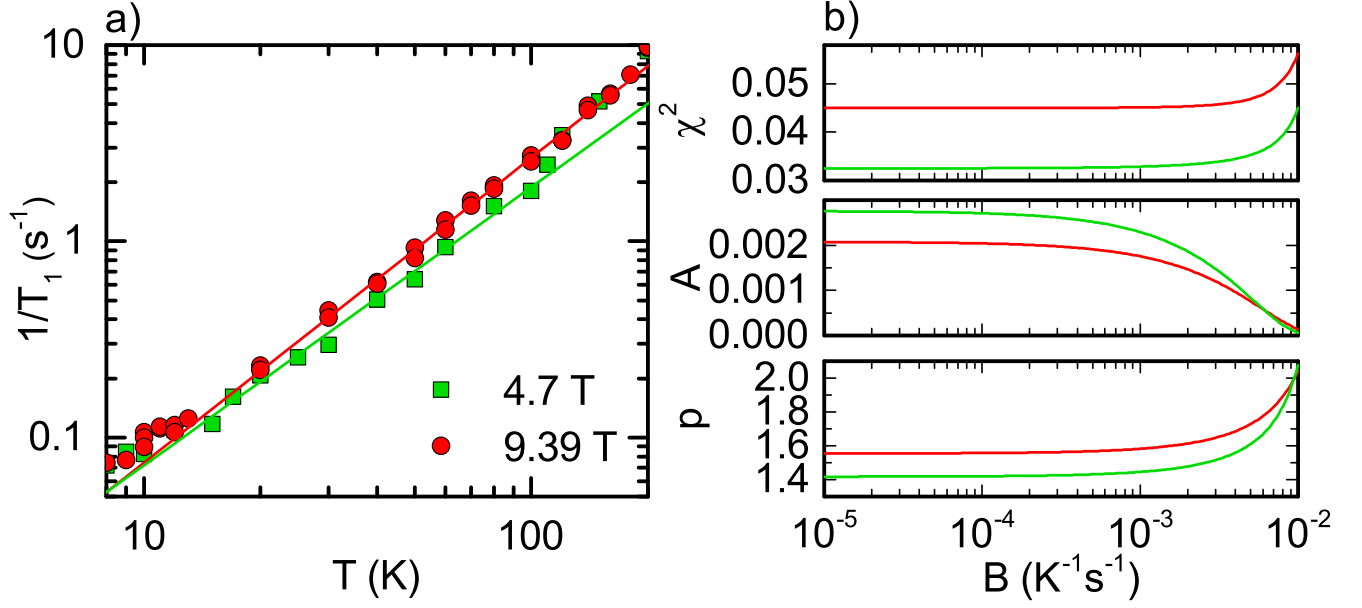


FIG. 3. a) ^{87}Rb spin-lattice relaxation rate $1/T_1$ measured in magnetic fields of 4.7 T (green squares) and 9.39 T (red circles). The data was fitted to a model $1/T_1 = AT^p + BT$ in the range 20 K – 100 K where we safely avoided possible non-universal regime (solid lines). The first term includes 1D TLL power-law dependence while the second stands for the 3D Korringa-type relaxation. With the only constraint $B > 0$, B converges to 0 in both fields ($B = 4.12 \times 10^{-18} \text{ K}^{-1}\text{s}^{-1}$ and $B = 4.68 \times 10^{-14} \text{ K}^{-1}\text{s}^{-1}$ respectively), meaning the 3D contribution is negligible. The corresponding A and p parameters are $A = 2.76 \times 10^{-3}$, $p = 1.42$ and $A = 2.07 \times 10^{-3}$, $p = 1.55$, respectively. b) χ^2 value of the fit (top), A and p parameters of the fit (middle and bottom) to $1/T_1 = AT^p + BT$ with different fixed B values. When B term becomes relevant, for $B > 10^{-3} \text{ s}^{-1}\text{K}^{-1}$, χ^2 rapidly worsens.

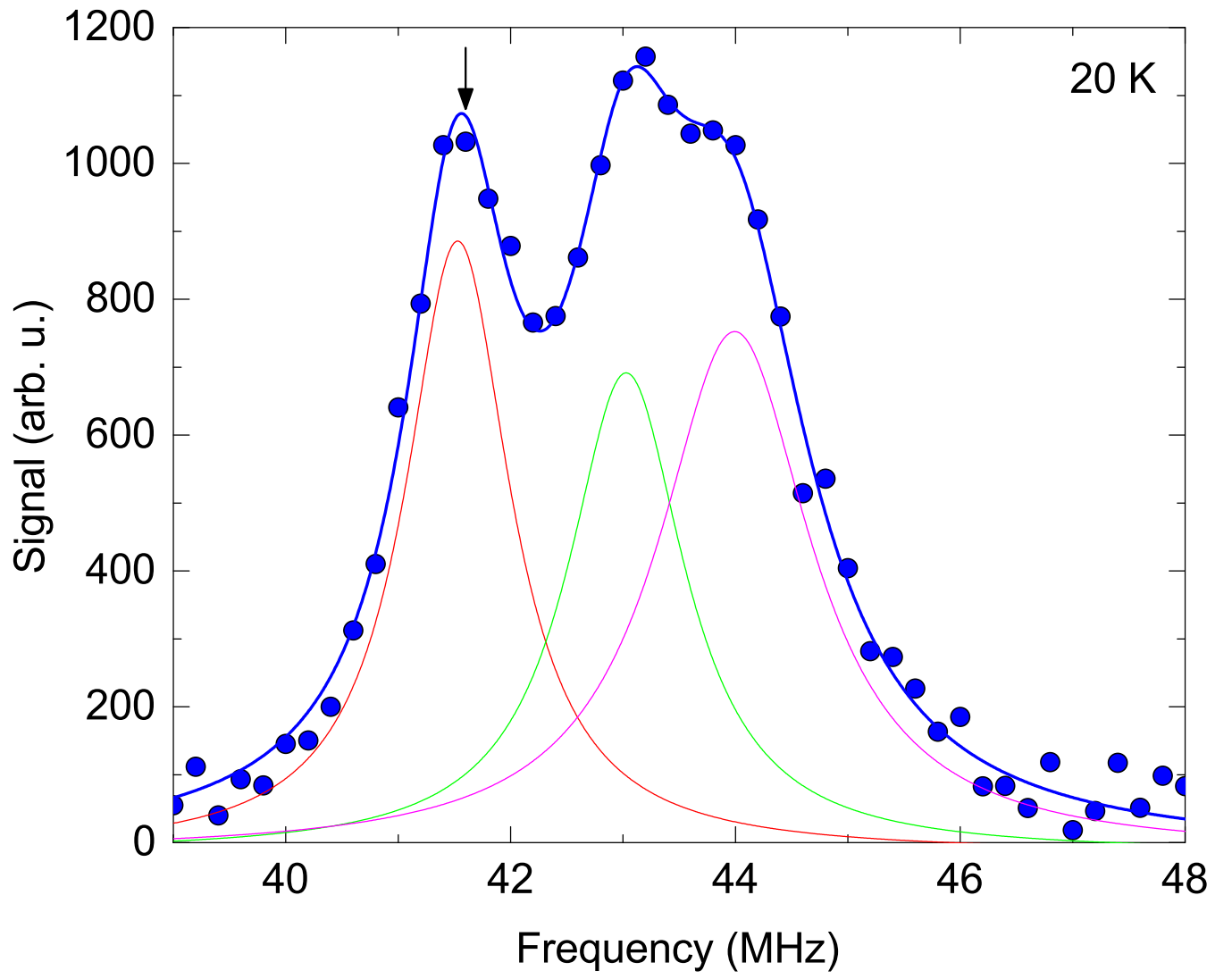


FIG. 4. ^{75}As NQR spectrum of $\text{Rb}_2\text{Mo}_3\text{As}_3$ powder measured at $T = 20\text{ K}$. Thin red, green and magenta lines are individual Lorentzian components used to deconvolute ^{75}As NQR spectra. Solid thick blue line is their sum. Arrow indicates the frequency at which spin-lattice relaxation rate measurements were conducted.

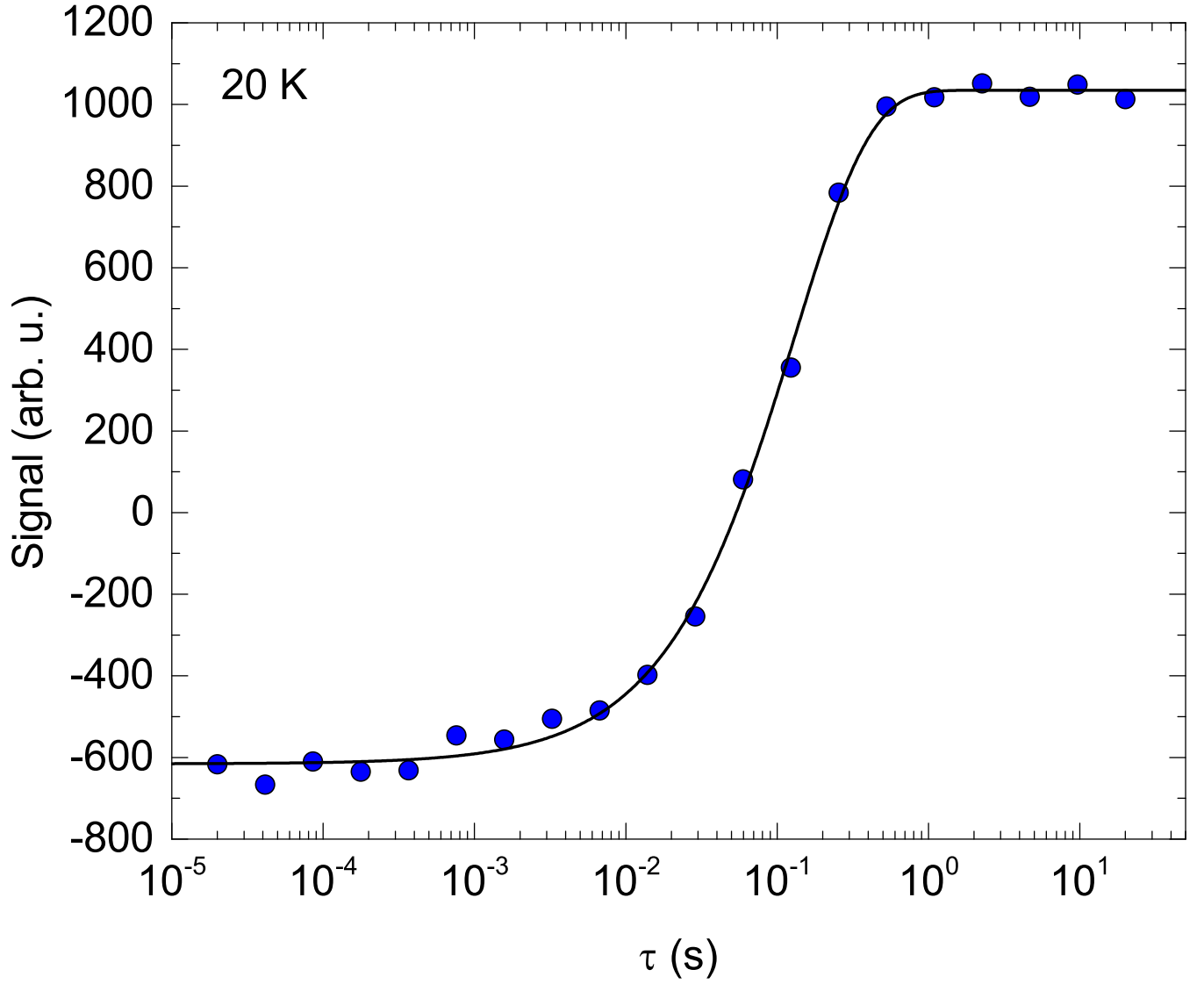


FIG. 5. The ^{75}As NQR signal intensity as a function of delay time τ in the spin-lattice relaxation rate measurements. Standard inversion-recovery pulse sequence $\pi - \tau - \pi/2 - \tau_1 - \pi - \tau_1 - \text{echo}$ (pulse lengths were typically $\pi/2 = 3.1 \mu\text{s}$ and the delay time $\tau_1 = 100 \mu\text{s}$) was used. The ^{75}As magnetization recovery curve was fitted to the expression for ^{75}As $I = 3/2$: $M_z(\tau) = M_0 (1 - (1 + s) \exp[-(3\tau/T_1)^\alpha])$. Here M_0 is the signal amplitude, s measures the efficiency of the nuclear magnetization inversion, and $\alpha \approx 0.9$ is the stretching exponent.